Korean J. Chem. Eng., 39(5), 1307-1315 (2022)
DOI: 10.1007/s11814-021-0992-0

pISSN: 0256-1115
eISSN: 1975-7220

The effect of chitosan (CS) coagulation bath on structure and performance of polylactic acid (PLA) microfiltration membrane

Fei Liu*, Bingbing Li*,†, De Sun*,†, Fenggang Li,†, Xinyue Pei***

*Department of Chemical Engineering, Changchun University of Technology, 2055 Yanan Street, Changchun 130012, P. R. China
**School of Chemical Engineering and Material Science, Zaozhuang University, Zaozhuang 277160, P. R. China
(*Received 17 April 2021 • Revised 9 October 2021 • Accepted 20 October 2021*)

Abstract−Membrane hydrophilicity is a crucial factor in evaluating ultrafiltration processes. In this paper, chitosan (CS) was selected for the hydrophilic modification of the polylactic acid (PLA) membrane, and PLA_{CS} membranes were prepared for the densification of the yeast solution. By non-solvent phase inversion method (NIPS), the PLA_{CS} microfiltration membranes were prepared by using chitosan (CS) acetic acid solution as the coagulation bath and glutaraldehyde as the crosslinking agent. PLA_{CS} membranes were characterized by water contact angle, porosity, pore size distribution, mechanical properties, ATR-FTIR, SEM, TGA and the ultrafiltration experiment. The viscosity of coagulation bath solution can severely influence the exchange rate of the solvent and the non-solvent as well during phase inversion; therefore, it can regulate the precipitation kinetics and membrane morphology. The results showed that chitosan (CS) was presented as granular on the pore surfaces of the PLA_{CS} membranes. When chitosan (CS) content increased, gel rate became smaller and membrane forming process was prolonged; the porosity and pore size of the PLA_{CS} were increased compared to the polylactic acid (PLA) membrane, pure water flux increased from 90.31 $L \cdot m^{-2} \cdot h^{-1}$ to 120.14 $L \cdot m^{-2} \cdot h^{-1}$, and yeast rejection rate increased from 75% to more than 90%.

Keywords: Polylactic Acid, Chitosan, Ultrafiltration Membrane

INTRODUCTION

It is well known that a very excellent biodegradable green environmental protection material, polylactic acid (PLA), is a linear aliphatic thermoplastic material derived from 100% renewable resources [1]. It can be prepared by the direct condensation of lactic acid and ring-opening polymerization of cyclic lactide, which is also called polylactide commercially. Cargill Dow LLC has developed a low-cost process for the continuous production of lactic acid-based polymers [2]. During polylactic acid (PLA) synthesis, corn is converted into glucose, and then lactic acid is obtained by fermentation of glucose, which is converted into lactide in the presence of a catalyst; after purification by vacuum distillation, the lactide is converted into PLA polymer by polymerization in the presence of a suitable catalyst [3].

As a natural polymer in renewable resources, chitosan (CS) can be extracted from shellfish and marine products of industrial waste. It has new characteristics, such as biocompatibility, biodegradability, antibacterial and wound healing activity. In addition, recent studies have shown that chitosan (CS) and its derivatives have the advantage of porous structure, coagulation bath formation, easy chemical modification, and high affinity for macromolecules in the body [4].

Membrane separation technology separates a mixture at molecular level through selectively permeable membrane. The semi-permeable membranes, with the walls full of small holes, can be divided into microfiltration membrane, ultrafiltration membrane, nanofiltration membrane, and reverse osmosis membrane, according to the pore size. Ultrafiltration means that when the separated components pass through the membrane under pressure, the solvent and low molecular weight solutes can easily pass through the membrane, and the relatively large molecular weight components are left on the surface of the separation membrane, so the mixed components are separated [5]. More and more scientists are using the phase inversion method to prepare ultrafiltration membranes with excellent performance. Rajaeian et al. prepared flat membranes by phase inversion and modified the membranes for hydrophilicity [6]. They also characterized their ultrafiltration performance. The modified separation membranes showed excellent permeation flux and anti-pollution performance. Zinadini [7] used nanoparticles to hydrophilically modify the separation membrane and produced a hydrophilic membrane with better performance. Compared with the unmodified separation membrane, the contact angle of the membrane is reduced and the anti-fouling ability is greatly improved. Ultrafiltration membrane water treatment technology has been widely used in environmental engineering work, and has played a good role in water treatment engineering.

At present, ultrafiltration membranes are prepared by polyethersulfone (PES), polyvinylidene fluoride (PVDF), and polyacrylonitrile (PAN) [8], but these materials are non-degradable, and the large number of waste ultrafiltration membranes formed a new white

†To whom correspondence should be addressed.
E-mail: lbingbing2002@163.com, sunde@ccut.edu.cn, LFGANG2005@163.com

pollution [9-11]. In this paper, polylactic acid, a degradable material, was used as membrane material, and chitosan, which is also degradable, was used for hydrophilic modification. Polylactic acid (PLA) and polylactic acid-chitosan (PLA_{CS}) membranes were prepared using water and chitosan (CS) acetic acid solution as coagulants. In the process of phase separation, chitosan was deposited on the inner pores wall of the membrane as particles. Meanwhile, due to the different contents of chitosan, the viscosities of the coagulation baths were different, which affected the exchange rate of solvents and non-solvents. Therefore, not only was the hydrophilicity of the prepared polylactic acid-chitosan (PLA_{CS}) membrane increased, but also the pore structure of the membrane was changed. Compared with polylactic acid (PLA) membrane, the porosity and pore diameter were increased.

EXPERIMENT

1. Materials

Polylactic acid (PLA) (imported 4032D) was obtained from American NatureWorks; Chitosan (CS) deacetylation degree ≥95%, viscosity 100-200 mPa·s and Glutaraldehyde (GA 25% aqueous solution) was purchased from Shanghai Maclean Biochemical Technology Co., Ltd and Tianjin Fuchen Chemical Reagent Factory, respectively. Porofil liquid was imported from Germany. Dry yeast food was bought from Changchun Xinli Food Co., Ltd. Deionized water was self-made in the lab. All chemicals used in this study were analytical grade without further purification.

2. Instruments

Precision electronic balance (JJ1000) and Electric heating constant temperature blast drying oven (DHG-9143BS-III) were obtained from American Shuangjie Brothers Co., Ltd. and Shanghai Xinmiao Apparatus Manufacturing Co., Ltd., respectively. Electronic outer diameter micrometer (0-150 mm), constant temperature heating magnetic stirrer (DF-101S) and rotational viscosity tester (NDJ-1) were purchased from Shanghai Constant Measuring Tool Co., Ltd., Jintan Kexi Instrument Co., Ltd. and Shanghai Ande Instrument Equipment Co., Ltd. Rotational viscosity tester (NDJ-1) and contact angle tester (Harke-SPCA) were provided by Shanghai Ande Instrument Equipment Co., Ltd. and Beijing Harke Test Instrument Factory. Porosimeter (Porolux 500) and scanning electron microscope (SEM: JSM-5500LV) were imported from Germany and Japan. Infrared spectroscopy (ATR-FTIR: Nicolet iS10) and thermogravimetric analyzer (TGA: STA 6000) were bought from the United States. Tensile tester (Shimadzu, AGS-X, 100 N) was imported from Japan.

3. PLA Membrane Preparation

First, PLA was vacuum dried at 60 °C for 48 h, then 6 g dried PLA was put into a three-necked flask and in 50 ml acetic acid added, heated to 80 °C in a water bath and stirred magnetically for 3 hours to obtain the homogeneous PLA casting solution; the solution was cooled to 60-65 °C and then scraped on a clean glass plate with a glass rod at room temperature with relative humidity 65%. After being exposed to air for 30 s, the glass plate with PLA membrane casting solution was immersed in the room temperature deionized aqueous solution for the gelling and solidifying to obtain the PLA membrane [12]. During this period, in order to obtain complete mass exchange between the casting solution and deionized water, the membrane needed to be soaked in deionized water for at least 24 hours, and the deionized water was replaced every 8 hours. After the exchange was complete, the obtained PLA membrane was carefully taken out, hung in a dust-free room temperature environment, and the PLA ultrafiltration membrane was obtained after complete drying.

4. PLA_{CS} Membrane Preparation

Different quantities of CS were added into the prepared 2% acetic acid solutions at room temperature [13-15], stirred for 5 h until chitosan was completely dissolved, then the crosslinking agent of 1% glutaraldehyde was added into above solutions [16]. The concentrations of chitosan acetic acid aqueous solutions were 0.25 wt%, 0.5 wt%, 0.75 wt%, and 1 wt%, and the mass ratio of glutaraldehyde to chitosan was 1.154: 100.

PLA casting solution was obtained by adding 6 g vacuum-dried PLA into 50mL acetic acid solution, heating it in water bath to 80 °C, stirring for 3 h until it was evenly dissolved, letting the PLA casting solution cool to 60-65 °C in atmosphere; then it was scraped on the glass plate with a glass rod in a stable humidity room temperature environment. It was put in the air for 30 s, the glass plate was immersed into chitosan acetic acid aqueous solution with the concentrations of 0.25 wt%, 0.5 wt%, 0.75 wt% and 1wt%, respectively, then named as $PLA_{0.25CS}$, $PLA_{0.5CS}$, $PLA_{0.75CS}$ and PLA_{1CS}, respectively.

5. Membrane Characterization

5-1. Gel Kinetics Test

The light transmittance of the membrane was tested using self-made light transmittance equipment. The curve of light transmittance and time can be used to analyze the precipitation rate of the casting liquid in the bath. The light transmittance experiments have been mentioned in many documents [17-19].

5-2. Water Contact Angle

Water contact angles (WCA) of the both sides of the membranes were tested at room temperature using HARKE-SPCA contact angle meter (Beijing Hakko test instrument factory). An appropriate amount of deionized water was injected into the syringe; in order to reduce the error, the water droplets were dropped on the upper and the lower surfaces of the membrane, respectively. Water contact angle was calculated by the dot-line method. The final result was the average of multiple tests.

5-3. Membrane Porosity

The sample membrane was cut into a square of 2 cm and wetted with the liquid of the Porofil. After the sample was completely wetted, it was taken out from the profile and weighed. Membrane porosity (ε) was investigated by gravimetric method described in the literature. The ε was calculated by the following equation:

$$\varepsilon = \frac{(m_w - m_D)}{\rho \times A \times \delta}$$

where, m_D is the weight of the dry membrane and m_w is the weight of the wet membrane, g; δ is membrane thickness, cm; A is the effective test area of membrane, m^2; ρ=1.87 g/cm^3 (Porofil liquid density).

5-4. Pore Size Distribution

To characterize the pore size distribution (PSD) and the mean pore radius (rm) of a membrane, a capillary flow porometer (Porolux

500, Germany) was employed using the wet/dry flow method [20]. First, membrane sample was wetted with the Porofil (a low surface tension wetting liquid), and then it was placed into a sealed chamber through which the nitrogen gas was flowed. The gas was forced to pass the flat membrane from the downside to the upside, and the pressure of the flowing gas was gradually increased and was recorded through flow simultaneously. When the pressure of the gas was high enough for the liquid to be removed from the largest pore, the size of the pore was recorded, which was the largest pore size (bubble point). With the increasing of gas pressure, the smaller pores became unblocked and caused an increase in the gas flow; when the whole membrane became dried, the pressure of the gas got to the cumulative. This highest pressure was used to calculate the pore size distribution and the average pore size. Non-cylindrical pores may have many diameters, but the wet/dry porometry method only measures one diameter per pore, that is the smallest diameter (throat). The average pore size (rm) and pore size distribution (PSD) of the sample membrane were measured using the capillary flow porosimeter and the dry/wet flow method.

5-5. ATR-FTIR

The ATR-FTIR was used to characterize the chemical structure of the membrane surface of each sample. The infrared test wavelength range was 4,000-500 cm^{-1}.

5-6. SEM

The scanning electron microscope was used to test the microscopic changes of the surfaces and the cross-section of the tested membrane. To test the cross-section, the membrane needed to be frozen to a certain extent in liquid nitrogen and then quenched.

5-7. TGA

Thermogravimetric analyzer was used to test the thermal properties of the sample membrane. The experiment was carried out in an inert gas N_2 atmosphere, and the temperature was increased from 30 °C to 500 °C at a rate of 10 °C/min, and the gas flushing was 50 mL/min.

5-8. Mechanical Properties

Membrane mechanical properties were obtained by a tensile tester with the loading velocity 20 mm/min at room temperature. To get an average value, at least three samples were tested.

5-9. Pure Water Flux and Rejection Rate

Fig. 1 is the test of pure water flux and yeast rejection rate of the

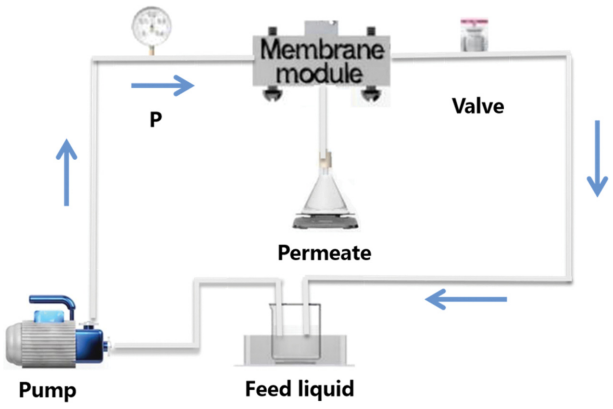

Fig. 1. Schematic set-up of ultrafiltration.

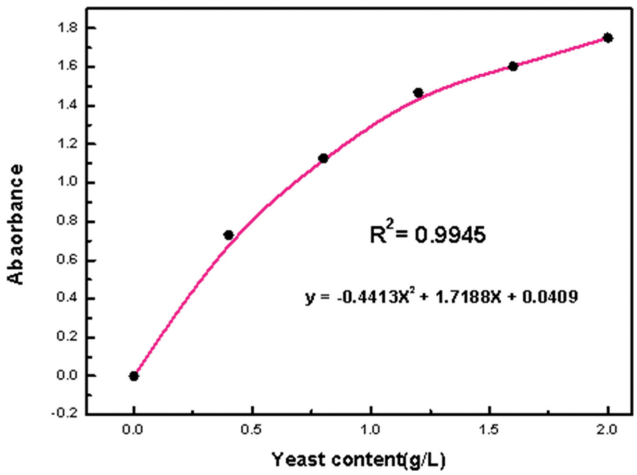

Fig. 2. Standard curve of 2 gL^{-1} yeast suspension at a wavelength of 600 nm.

sample membrane [21]. The effective area of the membrane was 0.000283 square meters, the pressure was 0.1 MP, the test temperature was room temperature, and the pure water flux test time after pre-pressing was 1 h. A comparison chart of the pure water flux was obtained. In this experiment, the yeast permeate was collected to calculate the yeast rejection rate. We used ultraviolet to test the absorbance of the permeate at 600 nm, and calculated the membrane retention rate of each sample through the yeast standard curve. Fig. 2 is the standard curve. Pure water flux (J) and yeast retention rate (R) algorithms are shown in the following formula:

$$J = Q/AT$$

$$R(\%) = (1 - C_p/C_f) \times 100\%$$

where, J represents pure water flux, L/m^2h; Q represents the volume of permeated liquid, L; A represents the effective area of the sample membrane, m^2; Δt represents the total permeation time, h; R represents yeast bacterial retention rate; C_p represents the concentration of the permeate, and C_f represents the concentration of the feed solution, in g/L, where the concentrations of the permeate and the feed solution are calculated by UV testing the absorbance of the permeate at 600 nm.

RESULTS AND DISCUSSION

1. Gel Dynamics

The phase separation of the casting liquid determines membrane permeability and membrane morphology. During the NIPS experiment, the interaction between non-solvent and polymer helps to increase the rate of phase separation between the solvent and the non-solvent, and the viscosity of the bath also affects the speed of the precipitation process of the membrane. Fig. 3 is the viscosity of the coagulation baths which had different CS dosages. The light transmittance experiment was used to analyze the membrane-forming mechanism of the casting liquids with water and chitosan acetic acid solution used as the baths. As shown in Fig. 4, all membrane formation belonged to instantaneous phase separation. The specific performance was that the light transmittance decreased rap-

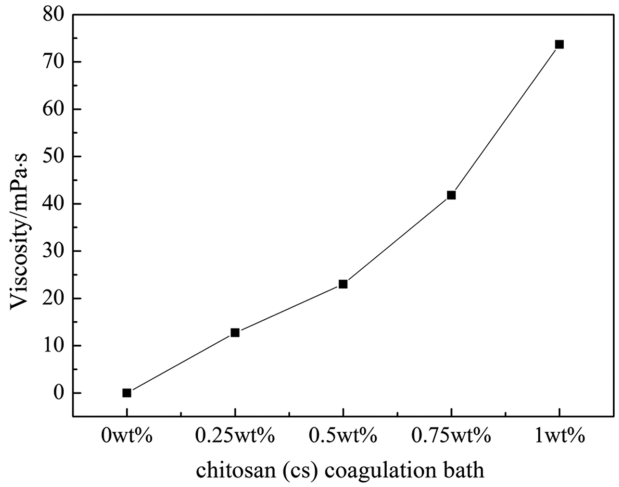

Fig. 3. Viscosity of coagulation bath with different CS dosages.

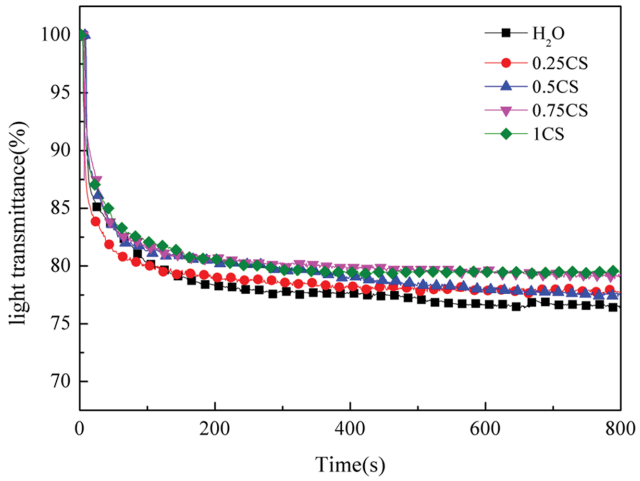

Fig. 4. Precipitation rates of casting solutions with different dosages of CS in coagulation baths.

idly with time at the beginning and then decreased slowly until the curve became stable, and the light transmittance value was not changed. It is obvious from the figure that the times for the light transmittance to stabilize were PLA>$PLA_{0.25CS}$>$PLA_{0.5CS}$>$PLA_{0.75CS}$>PLA_{1CS} in the order of time length. That is, the amount of CS in the bath became larger, and the time for the light transmittance to stabilize became longer. The main reason is that the higher viscosity of the bath will cause the precipitation rate of the casting liquid to decrease [22]. This in turn affected the final shape of the membrane.

In general, bath viscosity increases with the increase of the concentration of chitosan in the bath, and the change of the bath viscosity will affect the separation process. It is well known that for the membrane making process of NIPS, the rheological variation (i.e., viscosity) and the thermodynamic variation (i.e., the interaction between polymer and non-solvent) influence both the de-mixing rate and the de-mixing way of both the solvent and the non-solvent in casting solutions [23]. And when the viscosity of casting solution is low, the precipitation rate is fast [24,25], and the lower the viscosity is, the faster the precipitation will be. When the precipitation rate is fast, the light transmittance decreases rapidly, and the faster the precipitation rate is, the lower the light transmittance will be.

Table 1. Water contact angle of the membranes

Membrane	Contact angle of top surface (°)	Contact angle of bottom surface (°)
PLA	60.62	104.10
$PLA_{0.25CS}$	68.99	102.00
$PLA_{0.5CS}$	60.95	103.80
$PLA_{0.75CS}$	65.33	101.20
PLA_{1CS}	64.40	103.36

Table 2. Thickness (δ) and porosity (ε) of the membranes

Membrane	δ (μm)	ε (%)
PLA	132	76.78
$PLA_{0.25CS}$	114	76.74
$PLA_{0.5CS}$	115	77.53
$PLA_{0.75CS}$	117	78.54
PLA_{1CS}	119	81.40

2. Water Contact Angle

The water contact angle can reflect the water affinity of the solid material surface and whether the material is easily wetted by water. The smaller the water contact angle, the greater the affinity of the membrane surface to water and the better the hydrophilic performance. Table 1 displays the static contact angles of the PLA membrane and the $PLA_{0.25CS}$ to the upper and the lower surfaces of the membrane. It is not difficult to draw from the table that the water contact angle of the upper surface of the PLA membrane was 60.62°, the water contact angle of the lower surface was 104.1°, and the difference in water contact angles between the upper and the lower surfaces was 43.5°. The upper surface was hydrophilic and the lower surface was hydrophobic. As the CS content of the chitosan acetic acid solution increased, the contact angles of the upper and the lower surfaces of the PLA_{CS} membrane did not change much, and the hydrophilicities of the upper and the lower surfaces were almost the same as that of the PLA membrane.

3. Membrane Porosity

The ultrafiltration performance of the membrane is affected by the pore structure of the membrane [26]. Table 2 shows the thickness and the porosity of the membranes. The thickness of $PLA_{0.25CS}$-PLA_{1CS} decreased compared with PLA membrane, and the porosity increased with the increase of CS concentration of chitosan acetic acid solution. Since the water contact angles of the upper and lower surfaces of the PLA_{CS} membrane did not change much compared with that of the PLA membrane, the porosity tended to increase. Therefore, the change of the bath solution changed the internal structure of the membrane, that is, the gel rate decreased when the CS content increased. The membrane forming process is prolonged [27]. The membrane thickness obtained by NIPS method is related to the viscosity of the casting solution, which has little relation to the viscosity of the bath. Moreover, due to the same ratio of the casting solution, the difference in membrane thickness is

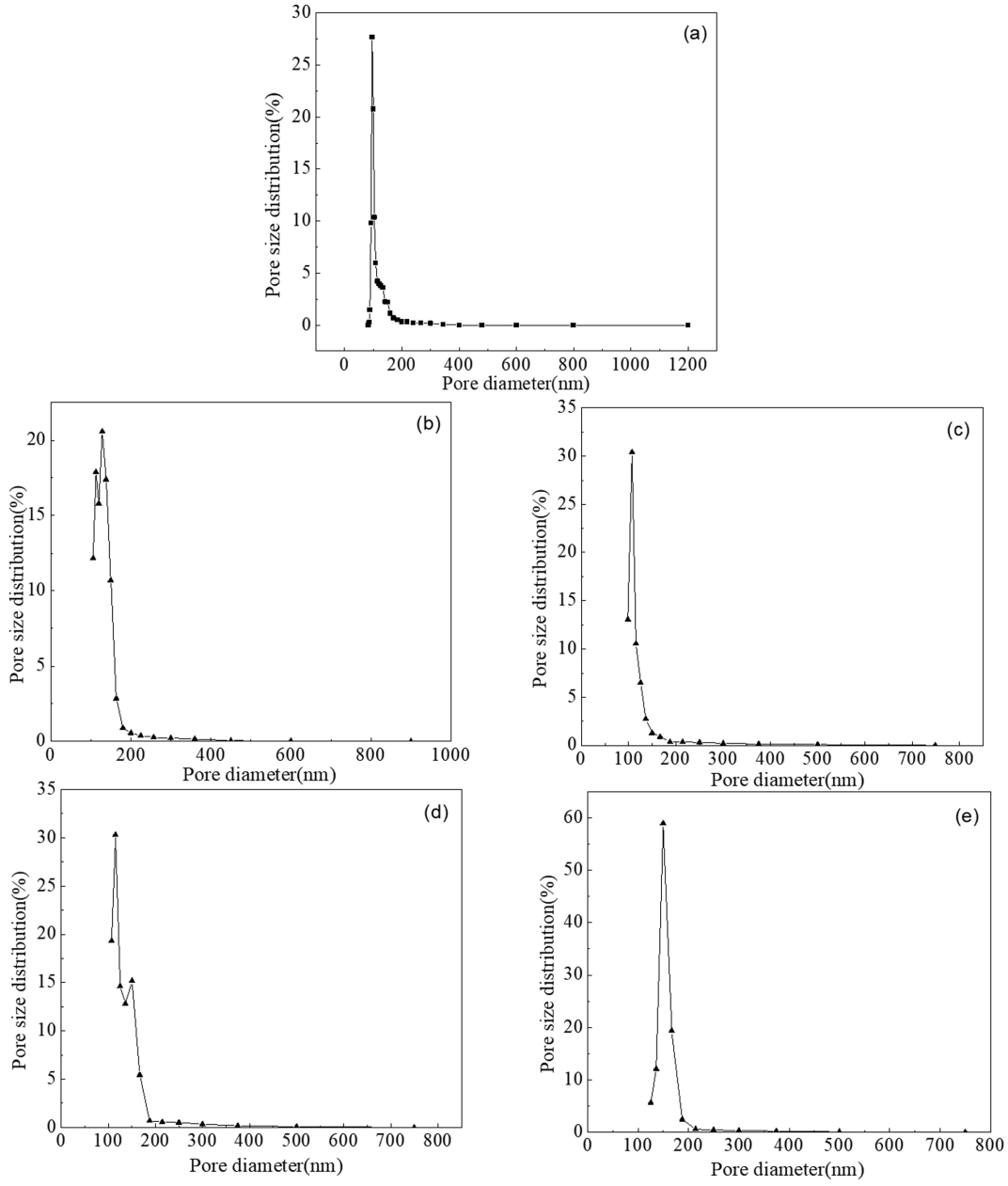

Fig. 5. Pore size distribution of the membranes. (a) PLA, (b) $PLA_{0.25CS}$, (c) $PLA_{0.5CS}$, (d) $PLA_{0.75CS}$, (e) PLA_{1CS}.

small. Through the test results, we can find that with the increase of the membrane thickness, the porosity decreased gradually.

4. Membrane Pore Size

The pore size distribution of the membranes is shown in Fig. 5.

Table 3. Pore size of the membranes

Membrane	r_s (nm)	r_m (nm)	r_b (nm)
PLA	**98.3**	**113.8**	**342.8**
$PLA_{0.25CS}$	105.9	115.8	599.6
$PLA_{0.5CS}$	98.47	120.8	748.8
$PLA_{0.75CS}$	107.1	125.6	749.3
PLA_{1CS}	200	160.2	1,375

The minimum aperture (r_s), the average pore size (r_m), and the maximum aperture (r_b) of the membranes are shown in Table 3. The pore size of PLA_{CS} was larger than that of the PLA membrane, mainly because chitosan acetic acid solution was used as the bath. The membrane structure was changed during the process, which can be seen through the cross-sectional view of the electron microscope. As CS concentration increased in the bath, the viscosity of casting solution became higher, the gel speed got slower, leading to a gradual increase in the pore size of the PLA_{CS} membrane.

5. ATR-FTIR Analysis

Fig. 6 shows the FTIR spectra of (a) pure PLA, (b) pure CS and (c) PLA_{CS} membranes. The characteristic peaks of pure PLA at around 2,945 cm^{-1} represent the stretching vibration of the asymmetric and symmetric peaks of C-H. The absorption peak at around 2,996

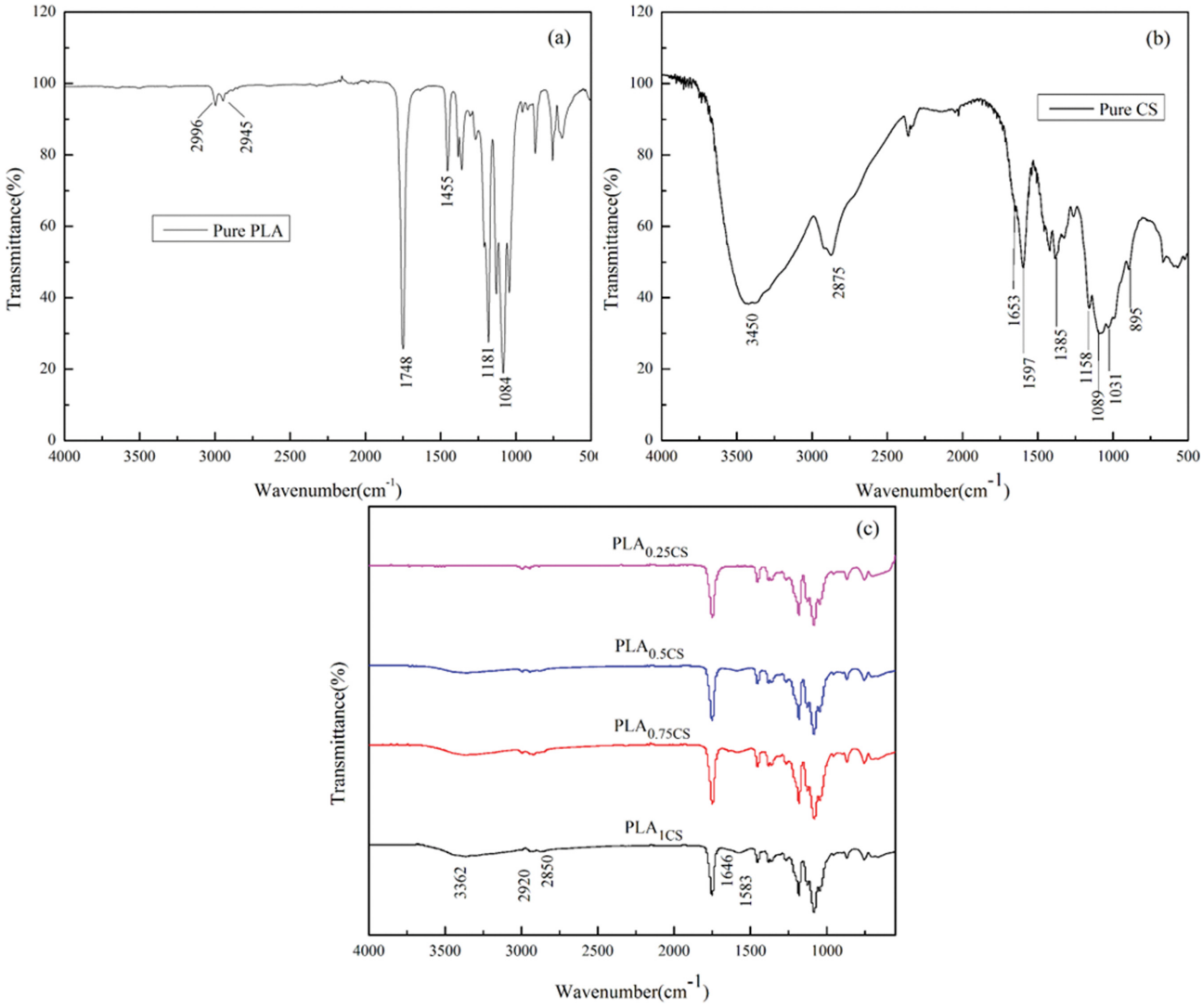

Fig. 6. FTIR spectra of the different dosage CS in coagulation baths.

cm^{-1} and 1,455 cm^{-1} corresponds to the stretching vibration of -CH3 in PLA membrane. The characteristic peak at 1,748 cm^{-1} is the C=O stretching vibration peak. The peak at 1,181 cm^{-1} cm is assigned to the dissymmetry deformation vibration of C-O-C, and the characteristic peak at 1,084 cm^{-1} is the C-O stretching vibration peak [28-30].

For CS infrared spectrum, the peak of 1,653 cm^{-1} is the C=O stretching vibration amide I peak, the peak of 1,597 cm^{-1} is -NH2 bending amide II peak, and the peak of 1,385 cm^{-1} is the bending vibration peak. C-O bonds at 896 cm^{-1}, 1,031 cm^{-1} and 1,089 cm^{-1} are the stretching vibration peaks that characterize the polysaccharide structure, while C-O-C glycoside bond at 1,158 cm^{-1} is the asymmetric stretching vibration peak [31]. In addition, O-H and N-H bonds at 3,450 cm^{-1} represent the wide stretching vibration peaks of intermolecular hydrogen bonds. 2,875 cm^{-1} is the bending vibration peak of -CH3 bond in $-NHCOCH_3$, and 1,385 cm^{-1} is the deformation vibration peak of -CH bond in $NHCOCH_3$ [32].

Compared with pure PLA, PLA_{CS} shows new O-H and N-H tensile characteristic peaks at 3,362 cm^{-1}, which are enhanced at 2,920 cm^{-1} and 2,850 cm^{-1}. The characteristic peak at 1,646 cm^{-1} is related to C=O tensile of amide I. The characteristic peak of 1,583 cm^{-1} was caused by the N-H bending of amide I [33]. After the bath changed from water to chitosan-acetic acid solution, stretching vibration peaks at 3,362 cm^{-1} of the O-H and N-H appeared, representing the intermolecular hydrogen bonds; in addition the peaks raised with the increasing of CS concentration.

6. SEM Analysis

Fig. 7 shows the morphological change of the upper and the lower surfaces, and the cross-sections of the PLA and PLA_{CS} membranes. Fig. 7(b) shows that the bottom surface of the membrane had a macroporous shape, which was similar to the bottom surface of the PLA membrane, but the pore size was larger. There were large cavities in the lower layer of the membrane. When water was replaced with different concentration chitosan acetic acid solutions, the gel rate of PLA casting solution decreased with the increase of CS concentration. A low gel rate will lead to the formation of sponge-like pores, while a high gel rate will lead to the formation of finger-like pores [26,34]. That is, for the PLA casting solution, water is a

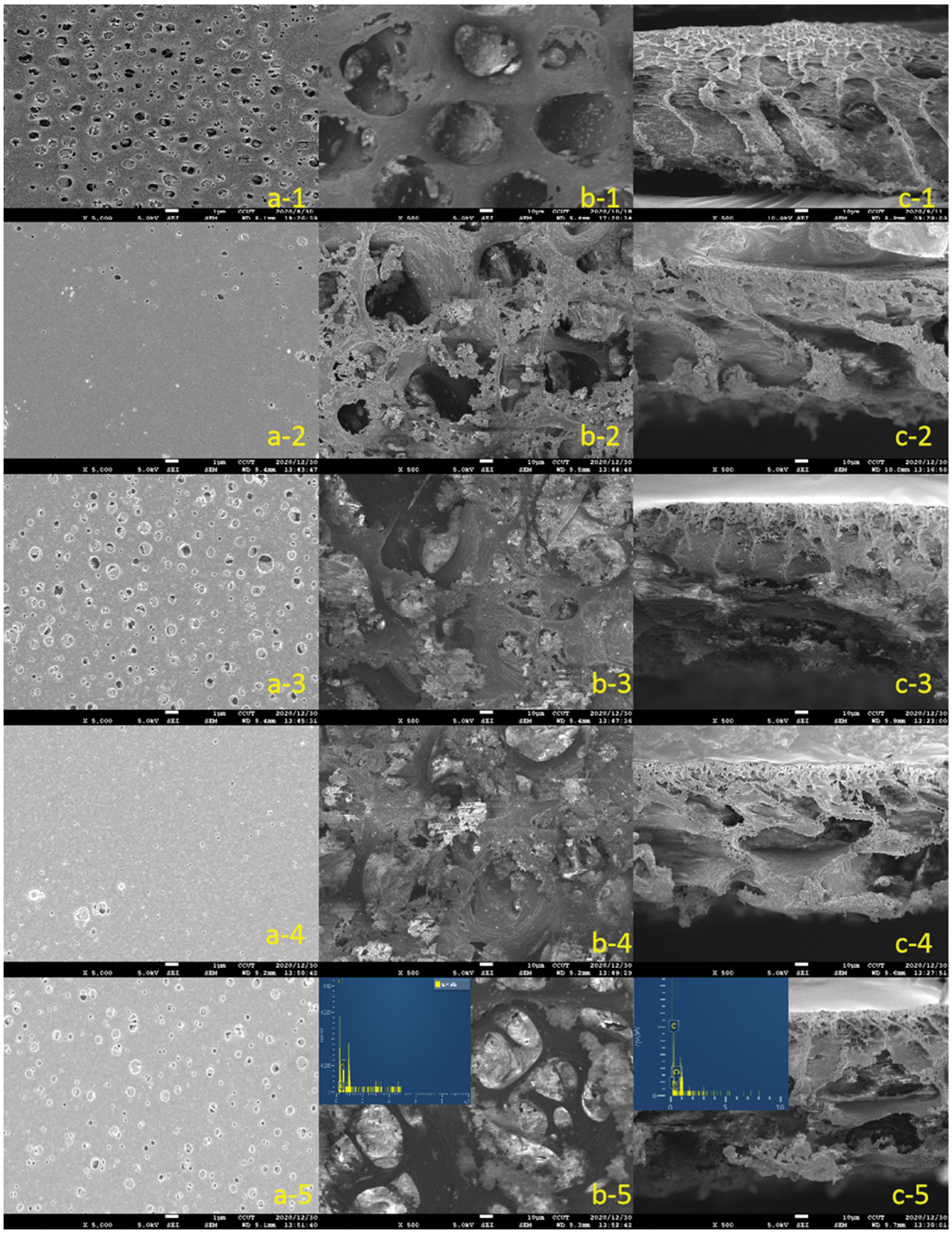

Fig. 7. SEM of membranes. (1) PLA, (2), $PLA_{0.25CS}$, (3) $PLA_{0.5CS}$, (4) $PLA_{0.75CS}$, (5) PLA_{1CS}. (a) Upper surface 5000×, (b) lower surface 500×, (c) section 500×.

strong non-solvent, and the chitosan acetic acid solutions of different concentrations are weak non-solvents compared to water. When the glass plate scraped with PLA casting liquid is directly put into the water bath, the phase separation occurs immediately, and the phase separation rate is very fast, thereby accelerating the rate of finger hole formation. However, scraping with the same PLA casting liquid, when the glass plate is immersed in the chitosan acetic acid solution of a weak non-solvent, the gel rate is reduced, which is not conducive to the formation of finger holes. The rate of finger hole formation slows as the concentration of chitosan acetic acid solution increases. From the above discussion, it can be concluded that the morphological structure of the membrane will change with the change of the concentration of the chitosan acetic acid solution in the bath, which in turn affects the permeability and selection performance of the membrane.

We performed elemental analysis for the bottom surface and the cross-section of the PLA_{1CS} membranes. From Table 4, only 6.49% nitrogen existed on the PLA_{1CS} membrane bottom surface;

Table 4. C, N, and O content on the bottom surface and the cross-section of the PLA_{1CS} membranes

PLA_{1CS}	C (wt%)	N (wt%)	O (wt%)	Total (wt%)
Bottom surface	67.77	6.49	25.74	100%
Cross-section	64.68	13.76	21.56	100%

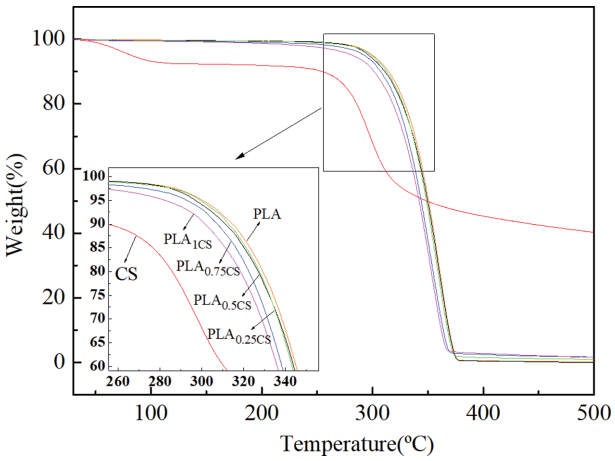

Fig. 8. TGA curves of different dosage of CS in coagulation bath.

Table 5. Mechanical properties of the membranes

Membrane	Tensile strength (MPa)	Breaking elongation (%)
PLA	2.8	8
$PLA_{0.25CS}$	0.87	4.2
$PLA_{0.5CS}$	1.29	5.5
$PLA_{0.75CS}$	1.82	6.0
PLA_{1CS}	2.02	6.4

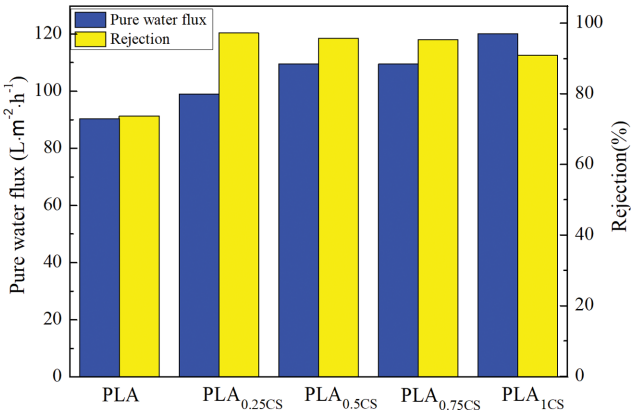

Fig. 9. Membrane pure water flux and yeast rejection rate.

however, there was 13.76% nitrogen on the cross-section of the PLA_{1CS} membrane. This can prove that the nitrogen of CS was more on the cross-section of PLA_{1CS} membrane, and CS was presented as granule on the pore surfaces of the PLA_{1CS} membrane.

7. TGA Analysis

Fig. 8 shows the thermal weight loss TG curve of the PLA_{CS} membrane, PLA membrane and CS. For the membranes of PLA and CS, the main weight loss stages can be seen from the figure. CS mainly had two obvious weight loss stages, the first stage mainly occurred at 50-150 °C, that water evaporated because of the hydrophilicity of chitosan. The second stage mainly occurred in the range of 220-400 °C due to the cleavage of the sugar ring and the degradation and depolymerization of the acetylated and deacetylated parts of the polymer [35,36]. The weight loss at this stage was about 50% of the total weight, and there was still nearly 40% of the weight undecomposed at 500°C. PLA had only one significant weight loss stage, which occurred in the range of 250-300 °C, indicating that the polylactic acid membrane had good thermal stability. The thermal stability of PLA_{CS} membrane also deteriorated due to the change of the bath. For the PLA_{CS} membrane, the corresponding temperature was lower than that of the base membrane when the weight losses were the same. This also shows that the thermal stability of PLA_{CS} membrane declined compared with PLA membrane. It is concluded that in terms of thermal stability, PLA membrane> PLA_{CS} membrane [37].

8. Mechanical Property Test

The tensile strength and elongation at break of PLA_{CS} and PLA membranes are shown in Table 5. For the PLA membrane, tensile strength decreased from 2.8 MPa to 0.87 MPa, and elongation at break decreased from 8% to 4.2%. For the $PLA_{0.25CS}$ membrane, the tensile strength increased from 0.87 MPa to 2.02 MPa, and the elongation at break increased from 4.2% to 6.4%. In the experimental range, the mechanical properties of PLA membrane were better than that of the PLA_{CS} membranes [38,39]. With the increase of CS concentration in the bath, the proportion of finger-like pores in the section structure of the membrane decreased, the proportion of spongy pores increased, and the mechanical properties of the PLA_{CS} membrane were improved.

9. Pure Water Flux and Rejection Rate

Generally, membrane pure water flux can be affected by the hydrophilicity of the membrane surface, pore penetration, pore size and porosity [27]. Fig. 9 shows the pure water flux and yeast rejection test results of the membrane of PLA and PLA_{CS}. Compared with PLA membrane, PLA_{CS} membranes had a great improvement in both pure water flux and yeast rejection. The pure water fluxes of PLA_{CS} membranes were increased compared with the PLA membrane, and the water flux was increased from 90.31 $L{\cdot}m^{-2}{\cdot}h^{-1}$ to 120.14 $L{\cdot}m^{-2}{\cdot}h^{-1}$; also the rejection rate was increased from 75% to 99%. With the increase of CS concentration in chitosan acetic acid solution, pure water flux increased gradually, while yeast rejection rate decreased gradually, and the membrane rejection rate with high water flux was relatively low. CS existed as particles on the inner surface of the aperture of the PLA_{CS} membranes, and it was hydrophilic, leading to an increase in flux. Because chitosan in granular form formed a rugged path in the pores, as yeast passed through the PLA_{CS} membrane pores, its interception rate was increased due to increased osmotic resistance.

CONCLUSIONS

Using water and chitosan acetic acid solutions as the baths, PLA

and PLA_{CS} membranes were prepared, the effect of the coagulation bath on membrane structure was discussed, and the basic process conditions for the preparation of the polylactic acid membranes were studied. Meanwhile, the basic performance of the membranes was evaluated through separation experiments. The main conclusions are as follows:

(1) When the bath was changed from water to CS acetic acid solution, the contact angles of the upper and lower surfaces of the PLA_{CS} membranes did not change significantly. The hydrophilicity was almost the same as that of the PLA membrane.

(2) With the change of the bath from water to CS acetic acid solution, the porosity of the PLA_{CS} membranes was increased. The change of the internal structure of the membrane indicated that the CS content increased, the gel rate became smaller and the membrane forming process was prolonged. With the increasing of the membrane thickness, the porosity decreased gradually.

(3) As CS concentration increased in the bath, the viscosity of casting solution increased and the gel speed decreased, generating a gradual increase in the pore size of the PLA_{CS} membrane.

(4) In the experimental range, the mechanical property of the PLA membrane was better than that of the PLA_{CS} membrane. With the increasing CS concentration in chitosan bath, the proportion of finger-like pores on the cross-section of the membrane decreased and the proportion of spongy pores increased. Meanwhile, the mechanical property of PLA_{CS} membrane improved gradually.

(5) Compared with PLA membrane, the pure water flux of the PLA_{CS} membrane increased and water flux increased from 90.31 $L \cdot m^{-2} \cdot h^{-1}$ to 120.14 $L \cdot m^{-2} \cdot h^{-1}$. The rejection rate of the PLA membrane was only 75%, and the PLA_{CS} membrane retention rate reached 90%, up to 99%, which was caused by the presence of chitosan particles on the inner surface of the aperture of the PLA_{CS} membranes. The change of the bath caused a change of the pore structure of the membrane.

ACKNOWLEDGEMENTS

Authors acknowledge the financial support from National Key R&D Plan under grant 2018YFB0504600, 2018YFB0504603, and the Foundation of Jilin Educational Committee (No: JJKH20191318KJ).

REFERENCES

1. P. D. Kiely, R. Cusick, D. F. Call, P. A. Selembo, J. M. Regan and B. E. J. B. T. Logan, *Bioresour. Technol.*, **102**, 388 (2011).
2. N. Saba, M. T. Paridah, M. Jawaid, K. Abdan and N. J. S. I. P. Azowa, *Agric. Biomass Based Pot. Mater.* (2015).
3. K. M. Villadiego, M. Tapia, J. Useche, *J. Polym. Environ.* (2021).
4 E. D. Freitas, C. F. Moura, J. Kerwald and M. M. Beppu, *Polymers*, **12**, 2878 (2020).
5. L. Hao, T. Zheng, J. Jiang, G. Zhang and P. Wang, *Chem. Eng. J.*, **292**, 163 (2016).
6. B. Rajaeian, A. Heitz, M. O. Tade and S. Liu, *J. Membr. Sci.*, **485**, 48 (2015).
7. S. Zinadini and F. Gholami, *J. Appl. Res. Water Wastewater*, **3**, 188 (2016).
8. G. D. Fan, Z. Y. Su, R. J. Lin, X. Y. Lin, R. X. Xu and W. Chen, *Int. J. Polym. Sci.*, **2016**, 1 (2016).
9. Q. D. Wu, A. Tiraferri, T. Li, W. C. Xie, H. Q. Chang, Y. H. Bai and B. C. Liu, *Acs Omega*, **5**, 23450 (2020).
10. N. B. Darwish, H. A. Abdulgader, H. Alromaih and A. Alalawi, *J. Water Process Eng.*, **27**, 32 (2019).
11. W. Wang, Y. P. Shi, P. Zhang, Z. C. Zhang and X. Xu, *J. Appl. Polym. Sci.*, **138**, 51165 (2021).
12. L. F. Padilha and C. P. Borges, *Braz. J. Chem. Eng.*, **36**, 497 (2019).
13. I. Bilican, S. Pekdemir, M. S. Onses, L. Akyuz, E. M. Altuner, B. Koc-Bilican, L. S. Zang, M. Mujtaba, P. Mulercikas and M. Kaya, *Acs Sustain. Chem. Eng.*, **8**, 18083 (2020).
14. J. F. Wu and L. Y. Zhang, *Int. J. Biol. Macromol.*, **121**, 1101 (2019).
15. J. D. Giraldo and B. L. Rivas, *Polym. Bull.*, **78**, 1465 (2021).
16. A. P. Shi, Y. Guan and Y. J. Zhang, *J. Bioact. Compat. Pol.*, **35**, 289 (2020).
17. J. Li, Z. i. Xu and Y. Hu, *Polym. Adv. Technol.*, **19**, 251 (2010).
18. D. Sun, M.-Q. Liu, J.-H. Guo, J.-Y. Zhang, B.-B. Li and D.-Y. Li, *Desalination*, **370**, 63 (2015).
19. Z. L. Xu, M. Liu, Y. M. Wei, L. B. Zhao and M. X. Xu, *Chem. Eng. Sci.*, **137**, 131 (2015).
20. M. Essalhi and M. Khayet, *J. Membr. Sci.*, **454**, 133 (2014).
21. C. W. Lee, S. D. Bae, S. W. Han and L. S. Kang, *Desalination*, **202**, 239 (2007).
22. P. K. Bajpai, I. Singh and J. Madaan, *J. Thermoplast. Compos. Mater.*, **27**, 52 (2014).
23. F. Xu, Z. Liu, J. Zhu, Q. Zhang and S. Li, *Appl. Surf. Sci.*, **266**, 368 (2013).
24. S. Devi, P. Ray, K. Singh and P. S. Singh, *Desalination*, **346**, 9 (2014).
25. L. B. Zhao, Z. L. Xu, M. Liu and Y. M. Wei, *J. Membr. Sci.*, **454**, 184 (2014).
26. H. P. Xu, W. Z. Lang, X. Yan, X. Zhang and Y. J. Guo, *J. Membr. Sci.*, **467**, 142 (2014).
27. J. O. Su, N. Kim and T. L. Yong, *J. Membr. Sci.*, **345**, 13 (2009).
28. M. S. Singhvi, S. S. Zinjarde and D. V. Gokhale, *J. Appl. Microbiol.*, **127**, 6 (2019).
29. W. H. Li, C. Zhang, H. Chi, L. Li, T. Q. Lan, P. Han, H. Y. Chen and Y. Y. Qin, *Molecules*, **22**, 1170 (2017).
30. G. Li, M. H. Zhao, F. Xu, B. Yang, X. Y. Li, X. X. Meng, L. S. Teng, F. Y. Sun and Y. X. Li, *Molecules*, **25**, 5023 (2020).
31. A. Avila, K. Bierbrauer, G. Pucci, M. Lopez-Gonzalez and M. Strumia, *J. Food Eng.*, **109**, 752 (2012).
32. S. Jiang, L. Jian, D. Man, Y. Li, H. Wang and S. Jiang, *Mater. Sci. Eng. C*, **59**, 86 (2016).
33. M. Haghbin, J. Esmaeilzadeh and S. Kahrobaee, *Macromol. Res.*, **28**, 1232 (2020).
34. M. Das and D. Chakraborty, *J. Appl. Polym. Sci.*, **102**, 5050 (2010).
35. A. K. Pal and V. Katiyar, *Int. J. Biol. Macromol.*, **95**, 1267 (2017).
36. T. C. Mokhena, J. S. Sefadi, E. R. Sadiku, M. J. John, M. J. Mochane and A. Mtibe, *Polymers*, **10**, 1363 (2018).
37. N. T. T. Trang, N. T. Chinh, N. V. Giang, D. T. M. Thanh, T. D. Lam and T. Hoang, *J. Electron. Mater.*, **45**, 3581 (2016).
38. L. X. Zhu, J. H. Qiu, W. D. Liu and E. Sakai, *Compos. Commun.*, **13**, 18 (2019).
39. M. M. Rahman, M. S. Islam and G. S. Li, *Polym. Test*, **68**, 302 (2018).